J. Micromech. Microeng. **21** (2011) 054013 (9pp) doi:10.1088/0960-1317/21/5/054013

Thermal fracture of oxidized polydimethylsiloxane during soft lithography of nanopost arrays

Wes W Tooley, Shirin Feghhi, Sangyoon J Han, Junlan Wang and Nathan J Sniadecki[1]

Department of Mechanical Engineering, University of Washington, Seattle, WA 98195-2600, USA

E-mail: nsniadec@uw.edu

Received 31 October 2010, in final form 29 January 2011
Published 28 April 2011
Online at stacks.iop.org/JMM/21/054013

Abstract

During the fabrication of nanopost arrays for measuring cellular forces, we have observed surface cracks in the negative molds used to replicate the arrays from a silicon master. These cracks become more numerous and severe with each replication such that repeated castings lead to arrays with missing or broken posts. This loss in pattern fidelity from the silicon master undermines the spatial resolution of the nanopost arrays in measuring cellular forces. We hypothesized that these cracks are formed because of a mismatch in the coefficient of thermal expansion (CTE) of polydimethylsiloxane (PDMS) and its oxidized surface layer. To study the fracture of PDMS due to thermal effects, we treated circular test samples of PDMS with oxidizing plasma and then heated them to cause surface cracks. These cracks were found to be more abundant at 180 °C than at lower temperatures. Finite element analysis of a bilayer material with a CTE mismatch was used to validate that thermal stresses are sufficient to overcome the fracture toughness of oxidized PDMS. As a consequence, we have ascertained that elevated temperatures are a significant detriment to the reproducibility of nanoscale features in PDMS during replica molding.

S Online supplementary data available from stacks.iop.org/JMM/21/054013/mmedia

(Some figures in this article are in colour only in the electronic version)

Introduction

Soft lithography is a set of manufacturing techniques for the fabrication of micro- and nanoscale structures [1]. It complements silicon-based fabrication techniques because it uses an elastic material, polydimethylsiloxane (PDMS), to replicate intricate features made in silicon or photoresist in a rapid and inexpensive manner [2]. Soft lithography is quite versatile in biological applications for it can be used to form fluid channels for biosensor platforms [3–5], flexible stamps for patterning biomolecules and cells [6], and topological surfaces for mimicking the native cellular environment [7]. PDMS is biocompatible and its surface can be functionalized with extracellular matrix proteins that facilitate the adhesion of cells and allow for their long-term culture on PDMS devices [8, 9]. Since PDMS is also mechanically flexible, it can be used to replicate arrays of posts for measuring cellular forces [10–13]. Recently, nanopost arrays have been produced, which provide better spatial resolution of cellular forces than micropost arrays due to the higher density of flexible PDMS post sensors underneath a cell (figure 1) [12].

PDMS is an organosilicon polymer that is synthesized from dimethylsiloxane oligomers with vinyl-terminated end groups, dimethylvinylated and trimethylated silica filler, a platinum catalyst, a cross-linking agent, dimethylmethylhydrogen siloxane, and an inhibitor, tetramethyltetravinyl cyclotetrasiloxane [8]. This mixture undergoes a hydrosilylation reaction which results in silicon-carbon bonding between the siloxane oligomers and silica filler to create a solid, elastic material. Heat is typically added

[1] Author to whom any correspondence should be addressed.

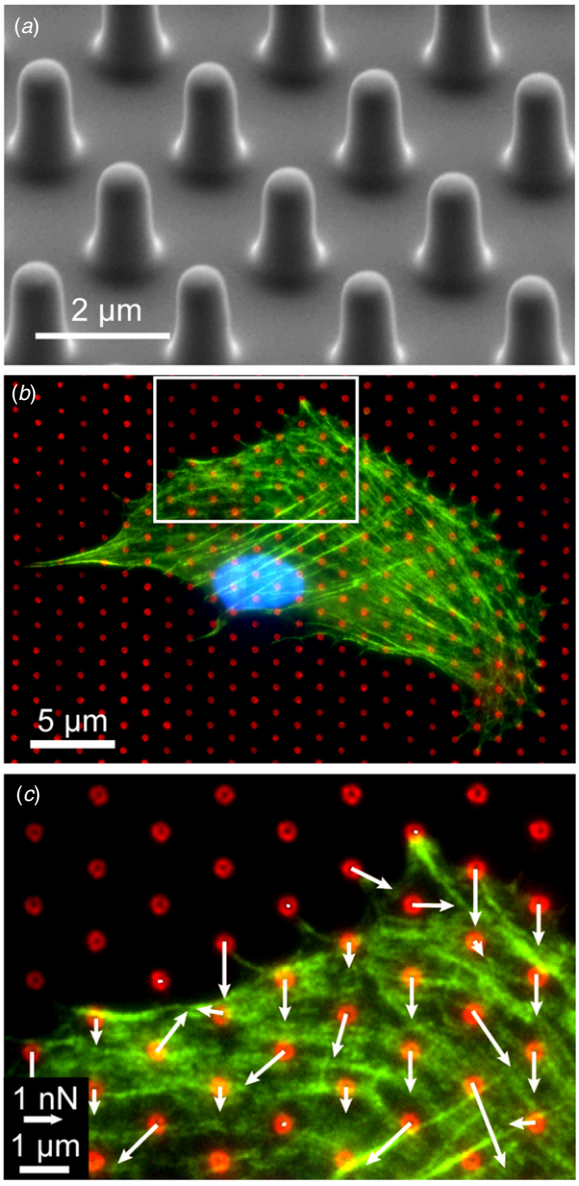

Figure 1. (*a*) SEM image of the PDMS nanopost array made by double-casting from a silicon master. (*b*) Immunofluorescence image of 3T3 fibroblast on the nanopost array (blue: DAPI; green: phalloidin; red: posts). (*c*) Traction force vectors were measured by analyzing the deflection of the nanoposts. This relationship is given by $F = (\frac{3}{4}\pi Er^4/h^3)\,d$, where F is the cell's traction force, E is the Young modulus, d is the deflection, r is the radius, and h is the height of the post.

during the organometallic cross-linking reaction to speed up the curing process. Once cured, the polymer has a coefficient of thermal expansion (CTE) of 3.1×10^{-4} K^{-1} [14–16]. The Young modulus of PDMS can range between 0.7 and 3.5 MPa, depending on the mixing ratio, curing temperature, and baking time [17–20]. The Young modulus of PDMS is lower than silicon-based or metallic materials and allows for it to undergo large elastic deformations during its removal from a master template with micro- or nanoscale features.

For the nanopost arrays, a double-casting process is used to replicate the arrays in PDMS from a single silicon master

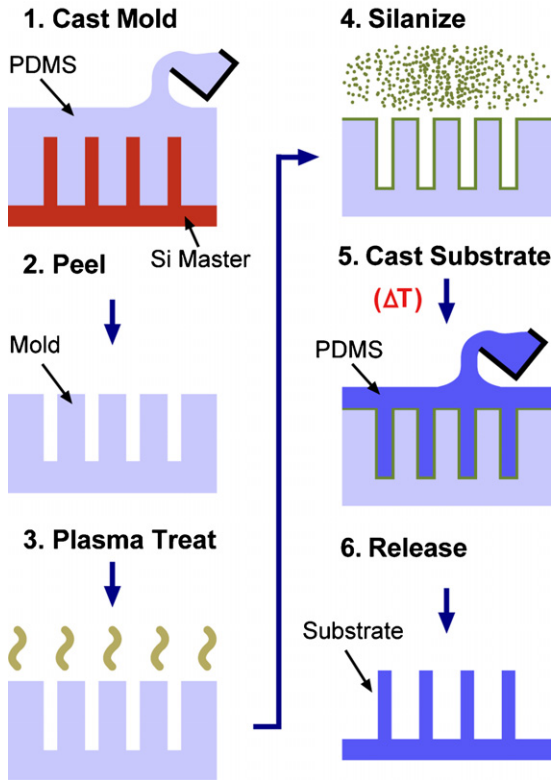

Figure 2. Schematic of the double-casting process to form nanopost arrays made from PDMS.

(figure 2). Several identical copies of the arrays are needed for experiments on cellular traction forces, so a fast and cost-effective replication process is needed [21]. During double-casting, uncured PDMS is cast against a master template with arrays of posts to create a negative that contains arrays of holes. The negatives are subsequently treated with oxidizing plasma to create silanol groups on the surface of the PDMS [22–24], which are then reacted with a fluorinated alkyltrichlorosilane to render a low surface energy coating on the negative [22, 23, 25]. Next, uncured PDMS is poured into the negatives, thermally cured, and peeled to release the newly formed arrays of posts. Although the double-casting process as described pertains specifically to arrays of posts, it has also been used to create patterns for stamps used in microcontact printing [25] and nanostructured topographies used to increase cellular adhesion [26].

During the double-casting process, we have observed surface cracks in the negative molds after casting (figure 3). These cracks are small and are generally considered a minor issue for soft lithography of microscale features. However, they raise a concern that soft lithography may have limits in replicating features at the nanoscale (figure 4). The existence of surface cracks in PDMS is well known and has been observed when PDMS is subjected to prolonged plasma treatments [27, 28], when stretched, plasma-treated, and released to cause the surface layer to buckle [29, 30], or vice versa when PDMS is plasma-treated and then stretched in order to fracture the surface [31, 32]. Plasma treatment of PDMS forms a brittle, superficial layer that is tens to

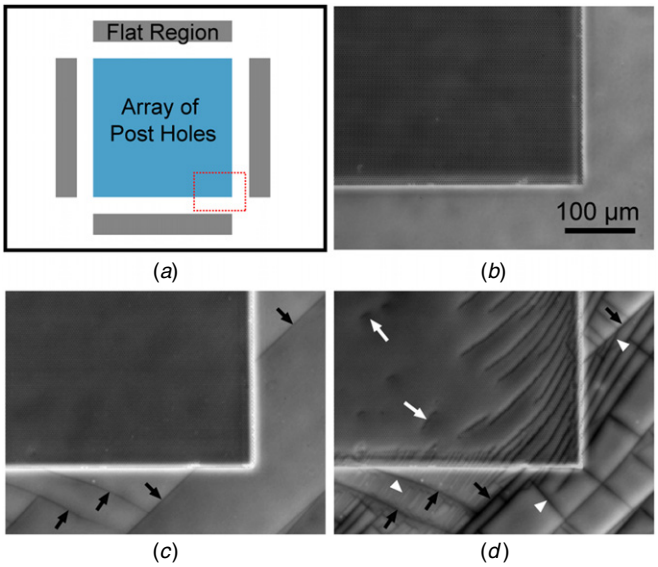

Figure 3. (*a*) Schematic diagram of the negative molds show that they contain arrays of holes that are surrounded by flat, rectangular regions with the same depth as the holes. (*b*) Phase contrast image of a negative mold before casting the post arrays. The surface of the negative has been plasma-treated and fluoro-silanized, but cracks were not observed on the surface. The same negative mold is shown after (*c*) two and (*d*) four castings. The black arrows indicate the cracks present after the initial casting, the white arrowheads indicate branching, secondary cracks, and the white arrows indicate *de novo* cracks.

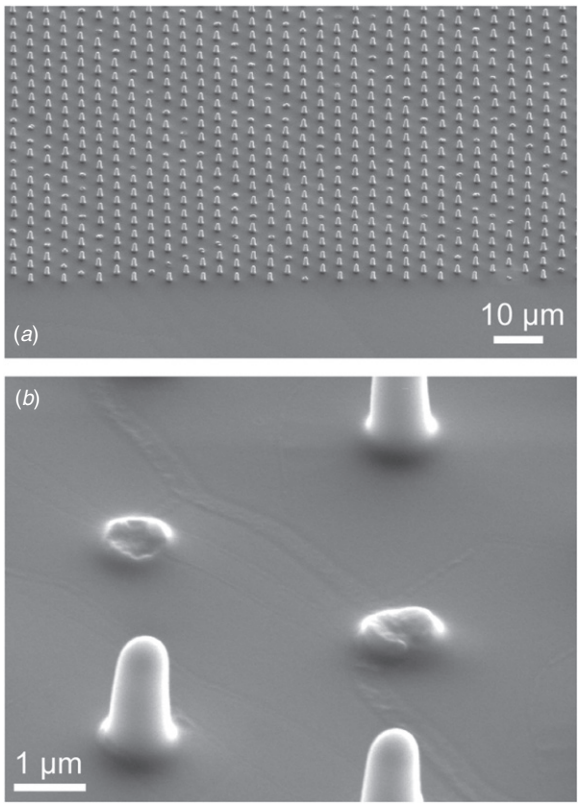

Figure 4. (*a*) SEM image of nanopost arrays cast from negative molds that had surface cracks. (*b*) SEM image of nanoposts show that surface cracks cause posts to be broken off and missing from within the array.

hundreds of nanometers in thickness and has a higher oxygen and lower carbon content than pure PDMS [28, 33, 34]. It is often referred to as a 'silica-like layer' even though its density and structure are not the same as pure silica [34]. Mechanical stress can be used to fracture the silica-like layer, but it has also been suggested that the cracks can arise from thermal stresses induced by a CTE mismatch between the underlying bulk PDMS and the silica-like layer [35].

In this study, we investigated the role of thermal effects in surface crack formation during the soft lithography replication of nanopost arrays. Previous studies on the fracturing of oxidized PDMS have focused on mechanically applied strains as the mechanism for crack formation [28, 33], but the role of thermal expansion in initiating surface cracks has not been well addressed. In the double-casting process, we observed that surface cracks accumulate with repeated use of the negative molds and tend to branch from pre-existing cracks. Subsequently, we adopted a testing method where circular test samples of PDMS were plasma-treated and then heated to induce thermal strains that initiated surface fractures. We found that increasing the heating temperature of the test samples led to a significant increase in the density of these cracks. To complement the experimental study, we performed a finite element analysis to approximate the maximum stress in the oxidized PDMS layer due to a CTE mismatch and confirmed that it was sufficient to induce fracture.

Materials and methods

Fabrication of PDMS posts

Uncured PDMS was prepared by mixing PDMS (Sylgard 184, Dow Corning) at a 10:1 ratio of the base to the curing agent and degassing under vacuum until all of the air bubbles were removed. Negative molds were formed by pouring PDMS over a silicon master template consisting of arrays of nanoposts. The fabrication of the silicon master has been described previously [12]. The negatives were cured for 10 min at 110 °C, and then peeled from the master template (figure 2). The negatives were subjected to 90 s of air plasma (Plasma Prep II, SPI supplies) at a pressure of 0.3 mbar, current of 100 mA, and power of 100 W and then silanized with (tridecafluoro-1,1,2,2-tetrahydrooctyl)-1-trichlorosilane (T2492-KG, United Chemical Technologies) in a desiccator under vacuum for over 14 h.

Once silanized, the negatives were used repeatedly to cast arrays of posts. The arrays were formed by pouring PDMS into the negatives and curing at 110 °C for 2 h. A plasma-treated glass slide was placed on top of the liquid PDMS before curing to create a rigid backing to the PDMS in order to aid in peeling. After each casting, the surface of the negatives was imaged under phase contrast microscopy (Nikon TiE) with a 10× objective and cooled CCD camera (Clara, Andor Technology) to identify cracks that arose during soft lithography. The orientation of each crack within the phase

contrast images was measured using custom-written code that used functions in MATLAB's image processing toolbox (Mathworks). The cracks were also analyzed using a scanning electron microscope (SEM) (FEI Sirion) that was operated with a working distance of 5 mm and a voltage of 5 kV. A film of gold-palladium was sputtered onto the negative molds to a thickness of approximately 7 nm before high resolution imaging.

To test whether the surface cracks affected the alignment and regularity of the nanoposts, arrays were cast from negative molds with no visible cracks and from negative molds that were severely cracked. The arrays were immunofluorescently stained with 5 μg ml^{-1} of DiI solution and their deflections were analyzed as previously described [12, 13]. Briefly, the average displacement per post was measured for each array by comparing the top and bottom centroid position of the nanoposts. This analysis was used to determine whether the nanoposts were distorted as a result of surface cracks.

Circular PDMS test samples

Uncured PDMS was prepared as described before and cast for 1 h at 110 °C between two fluoro-silanized glass plates. Spacers made from 1 mm thick glass slides were placed between the glass plates to maintain a consistent PDMS sheet thickness. An American standard paper hole puncher was used to cut 8 mm diameter test samples from the PDMS sheet. The top surfaces of the test samples were cleaned with Scotch® adhesive tape to remove dust and debris. The test samples were then placed onto a glass slide so that they could be transported and inspected. Plasma treatment of the surface of the test samples was performed as described previously. The samples were then heated in gravity convection ovens at 150 or 180 °C for 1 h and allowed to cool before imaging the induced surface cracks with phase contrast microscopy.

To quantify the density of the cracks on the surface of the test samples, phase contrast images were taken at four cardinal points along the perimeter of each of the samples: north, south, east, and west. Image analysis of the density of the surface cracks in the collected images was conducted using a custom-written code in MATLAB. Specifically, each image was binarized by thresholding above 33.3% of the maximum pixel intensity for the samples heated to 150 °C and 16.9% for the samples heated to 180 °C. The two threshold values were found by trial-and-error in order to achieve a faithful segmentation that partitioned out the surface cracks from the visible debris in the PDMS or optical obstructions in the light path from the microscopy objective to the camera. Once binarized, the crack density in each image was quantified by dividing the number of pixels for the cracks by the total number of pixels in the image. The results of the image analysis were statistically compared with Student's *t*-test.

Finite element modeling

A two-dimensional finite element model of a bilayer material consisting of a thin silica-like top layer and a PDMS base layer was constructed in ANSYS 11.0 (figure 10(*a*)). The two-dimensional model was a simplification of the three-dimensional circular PDMS samples because a circular disk can be described mathematically as a rectangular shape that is revolved about a central axis. The top layer was modeled with a thickness of 50 nm, which we based upon the depth of the cracks we measured using atomic force microscopy (dimension 3100 AFM). Simulations were run with a Young's modulus value that was varied between 10 MPa and 70 GPa, which are within previous estimates for oxidized PDMS [20, 29, 30, 33, 34, 36]. Additionally, Poisson's ratio of 0.2 and CTE of 0.55 $\times$ 10^{-6} K^{-1} were used for the silica-like layer since they are typical values for silica glass materials [37]. The underlying PDMS layer was given a thickness of 1 mm, Young's modulus of 3 MPa, and Poisson's ratio of 0.499, since PDMS can be assumed to be an incompressible material. The CTE value used for PDMS was 3.1 $\times$ 10^{-4} K^{-1}, which we verified by measuring the change in length of PDMS samples in an oven at elevated temperatures. The boundary condition at the top surface was modeled as a free surface that could expand under thermal effects, while the bottom surface was modeled with a fixed boundary condition due to adhesion and friction with the underlying glass slide. One end of the bilayer material was assigned a free surface boundary condition, while the other end was given a symmetric boundary condition since it was coincident with the central axis of revolution. A finite element mesh using quadratic, solid, eight-node elements (PLANE183) was constructed. A temperature rise of 90 or 160 K was imposed on the model to induce thermal expansion. The stress in the radial direction in the silica-like layer was reported since it causes mode I fracture. Convergence in the result of each simulation was confirmed using multiple meshing densities.

Results and discussion

Surface cracks increase with repeated castings

Arrays of nanoposts were cast repeatedly from the same negative mold to create identical PDMS replicas of a silicon master. Four flat, rectangular regions surround each array of nanoposts and acted as stiff, support structures to prevent the posts from buckling during microcontact printing (figure 3(*a*)) [10, 12, 21]. Phase contrast images of the negatives before casting the post arrays, but after plasma treatment and fluoro-silanizing, showed that there were no visible cracks on the surface of the negatives (figure 3(*b*)). After casting, however, cracks were seen to span the surface of the negatives and grew worse with additional replications (figures 3(*c*) and (*d*)). The black arrows indicate the initial cracks that formed on the negative which remained present throughout the mold's lifetime of usage. Under phase contrast, these cracks appear to be darker and more pronounced with additional replications.

Once a crack had formed, it could act as an initiation point for new cracks. The white arrow heads indicate secondary cracks which arise after the initial cracks and intersect with them. It is likely that the initial cracks provide pre-crack defects or act as stress risers for the secondary cracks. The

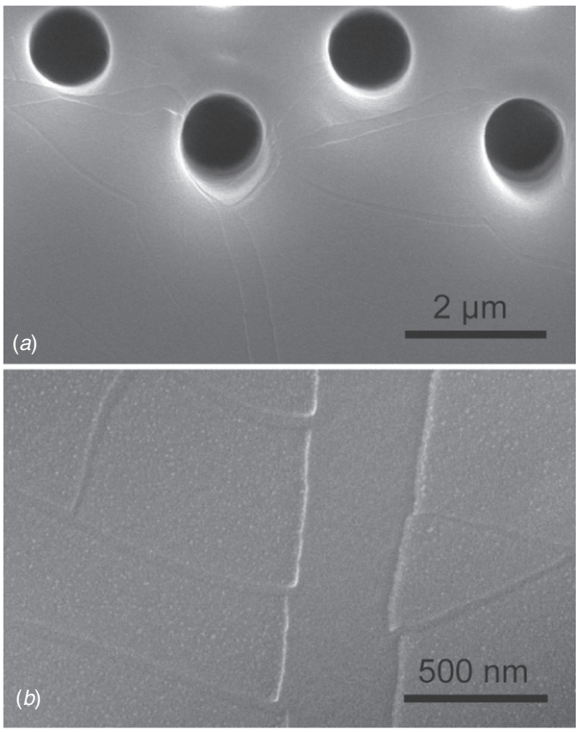

Figure 5. (*a*) SEM images show that cracks form after the first casting with the negative mold. The cracks were present near the holes in the negative mold but were not seen on the walls of the holes. (*b*) SEM image of a wide surface crack with smaller branching cracks.

formation of cracks within the array of post holes was much less common than in the surrounding regions. They tended to arise after several replications and were seen to form *de novo* and end abruptly (white arrows). Additionally, cracks that started in the surrounding regions were seen to propagate across the array of holes. These cracks appeared jagged and were seldom seen to generate branching, secondary cracks. The presence of cracks within the array of holes is a major concern as they can cause posts to break off at their bases, which undermines the spatial resolution of the arrays (figures 4(*a*) and (*b*)).

Surface cracks are wide and shallow

In an attempt to better understand the dimensions of these surface cracks and the resulting implications for fabricating nanopost arrays, negative molds were imaged with a SEM after a single casting (figure 5). The cracks that formed during the first castings had widths up to 500 nm, while the branching cracks had widths that were on average 50 nm (figure 5(*b*)). These values fall within the ranges seen previously when surface fracture was induced on plasma-treated PDMS samples [31–33]. The cracks found near the array of holes were seen to split and deviate around the edge of the holes, or in some instances, a crack was seen to intersect with a hole (figure 5(*a*)). From the samples examined, surface cracks were confined to the regions between the posts and the cracks did not propagate down the walls of the holes. Even though the holes can act as stress risers and cause fractures in their local vicinity, they

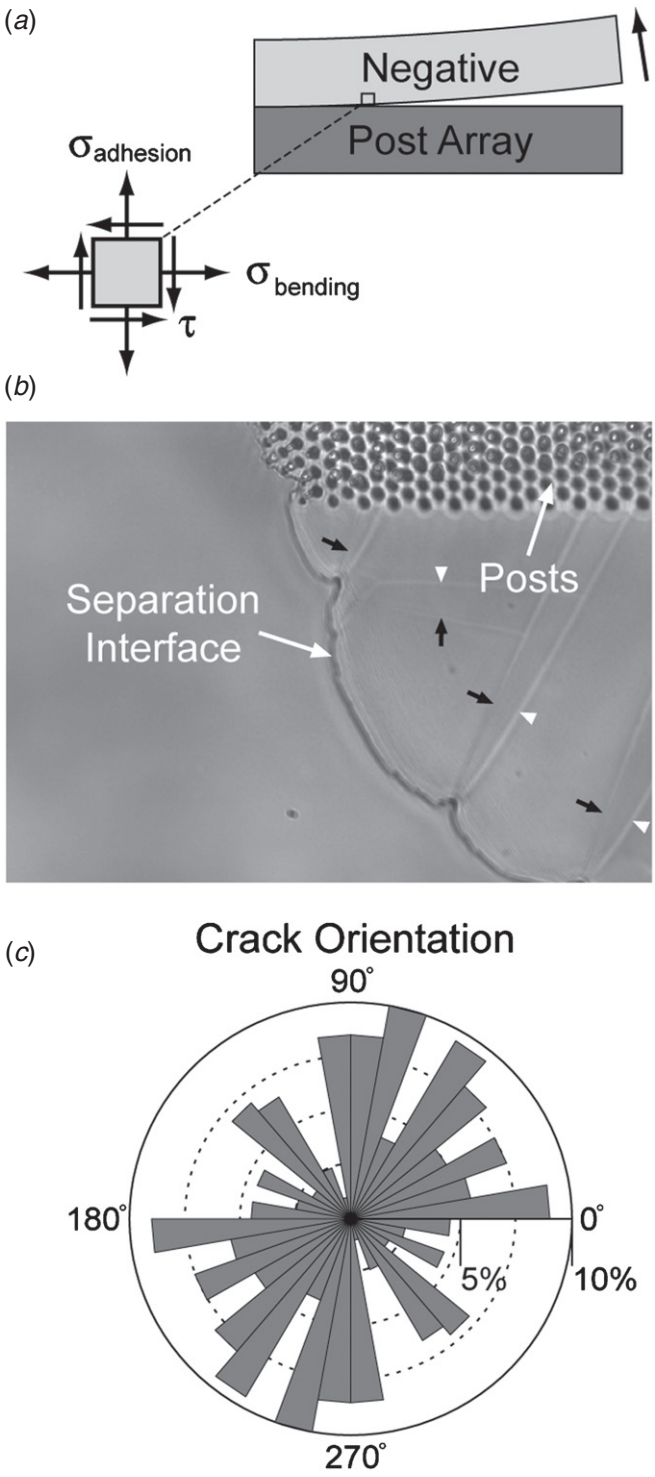

Figure 6. (*a*) Diagram of the stresses at the separation interface in the negative mold during the peeling process. (*b*) Phase contrast image taken during peeling of the post arrays from the negative mold. Surface cracks in the negative (black arrows) are seen to be aligned perpendicular to the peeling interface. Replicated crack-like features are seen on the cast post arrays (white arrowheads). A video of the peeling process is available in the supplementary data at stacks.iop.org/JMM/21/054013/mmedia. (*c*) Angle histogram plot of crack orientation on a negative mold.

also act to impede the growth of cracks [38]. A crack that intersects a hole is less likely to grow in length because the

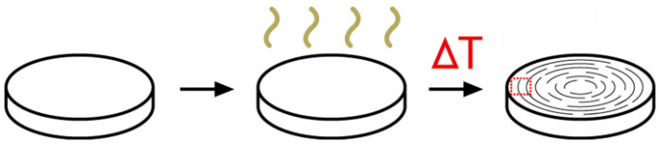

Figure 7. Schematic of inducing thermal fractures on PDMS test samples. A circular section is cut from a sheet of PDMS and its surface is treated with oxidizing plasma. The sample is then heated, causing the formation of concentric surface cracks. The dashed region indicates one of the four cardinal points along the perimeter that was imaged under phase microscopy for each sample.

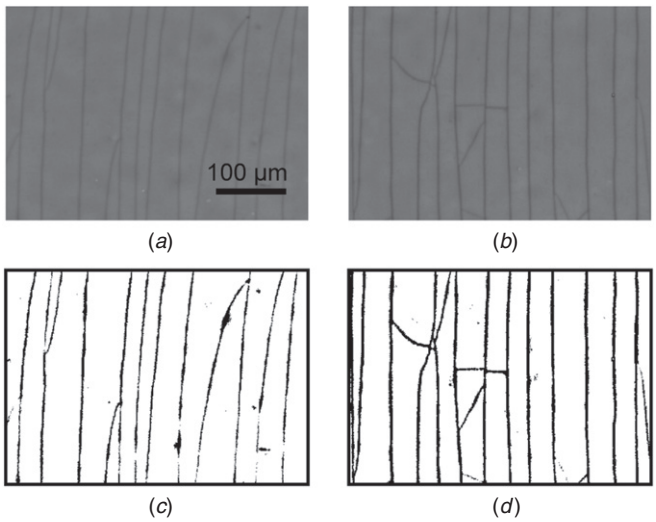

Figure 8. (*a*), (*b*) Phase contrast image of thermally fractured PDMS test samples heated at 150 and 180 °C, respectively. (*c*), (*d*) Binarized image of the phase contrast images. The pixel count for each image was used to calculate the surface crack density.

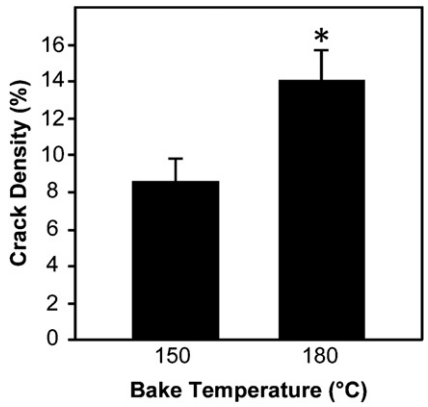

Figure 9. Surface crack densities in test samples increase with temperature. Quantification of crack density was conducted in MATLAB for phase images taken at four cardinal points at the perimeter of each sample ($N = 4$ for each temperature analyzed). The error bars represent standard deviation in the 16 images. The asterisk denotes $p < 0.01$ (Student's *t*-test).

infinitely small radius of curvature of its tip becomes the radius of the hole it intersects. This is analogous to the effect of small holes that are drilled in high strength materials to arrest the growth of cracks by blunting the sharpness of its tip.

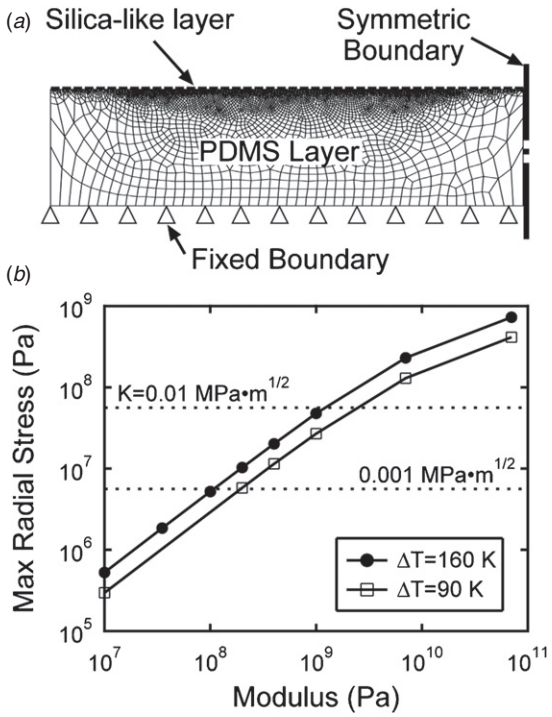

Figure 10. (*a*) Finite element model of thermal expansion of PDMS with a silica-like layer. (*b*) Simulated maximum radial tension as a function of Young's modulus of the silica-like layer for a temperature change ΔT of 90 and 160 K. The horizontal dashed lines indicate the stress required to overcome the fracture toughness K of the silica-like layer for a 10 nm pre-crack defect.

The inspection of the nanopost arrays under the SEM showed that the dimensions of the height and length of the posts are relatively unaffected by the surface cracks (figures 4(*a*) and (*b*)). Additionally, we compared nanopost arrays cast from severely cracked negative molds with arrays cast from molds without any visible cracks to determine whether the nanoposts remained perpendicular to the surface of the array. If cracks in the negative molds caused the nanoposts to be tilted or distorted, then they would not be suitable for measuring cellular traction forces because they would give a false reading of the local traction force of a cell. By comparing the centroid positions of the top and bottom of nanoposts within the arrays, the average displacement per post was calculated and found to be statistically indistinguishable: 77 ± 56 nm for arrays from severely cracked molds versus 85 ± 72 nm for arrays from uncracked molds ($p > 0.23$, Student's *t*-test). Thus, the surface cracks lead to wear and tear on the negative molds that ultimately cause missing posts within the arrays.

The images of dark cracks from phase contrast microscopy in figure 3 are likely an effect of optical diffraction [39]. We deduce that the cracks appear to be more pronounced because the surface topology at a crack causes the optical path of the phase light to be diffracted. The SEM images were inconclusive as to the source of fracture; no defects or debris were seen at the surface of the negatives that could initiate the formation of cracks. Moreover, the cracks were seen under the SEM to remain open after their formation. This would suggest that the underlying PDMS layer is in compression

and the silica-like layer is in tension. Once fracture occurs, the mismatch in stress between the layers is alleviated and the silica-like layer moves apart, while the underlying PDMS expands back to its stress-free state.

Cracks do not arise due to peeling

It is debatable whether the process of peeling the nanopost arrays from the negative molds could cause surface cracks. We note that, in general, tensile stresses acting in a perpendicular direction to a crack can increase its length by opening it under mode I fracture. The applicability of this mode of fracture for oxidized PDMS is supported by previous studies where tensile stresses were used to create nanogrooves or nanochannels, since these cracks were formed perpendicular to the applied stress [31, 32]. Additionally, compressive stresses used to buckle the silica-like layer of PDMS also caused cracks that were perpendicular to the direction of the wrinkles [29, 30]. These cracks arise from Possion's effect where compression causes tensile strain in the perpendicular direction. Thus, these examples strongly support that tensile stress causes the brittle silica-like layer of PDMS to fracture.

In analyzing the stresses that arise during peeling, we considered three kinds of stresses acting on the surface of a negative mold: a tensile normal stress from the adhesion energy between the negative and the array (σ_{adhesion}), a tensile bending stress from flexing the negative mold away from the array (σ_{bending}), and a shear stress from sliding the negative against the array (τ) (figure 6(*a*)). The direction of σ_{adhesion} and τ would cause cracks that penetrate underneath the silica-like layer and delaminate the oxide layer from the bulk PDMS. Since we did not observe delamination of the negative molds, the influence of these stresses can be considered to be negligible. The direction of σ_{bending} would cause cracks to form that are perpendicular to the direction of pealing, or in other words, aligned parallel to the separation interface. Cracks with this alignment were seldom observed (figure 6(*b*)). When the directions of the surface cracks in a negative mold were analyzed, their orientations were distributed widely and a strong preference in the direction was not observed (figure 6(*c*)). Thus, the randomness in the direction of the cracks indicates that peeling does not cause the surface fractures.

Video microscopy of the peeling process can provide an additional insight into the origin of the cracks (available in the supplementary data at stacks.iop.org/JMM/21/054013/mmedia). While observing the separation of the array from the negative mold during the peeling process, the separation interface tended to form a trailing meniscus along the length of the cracks. One explanation for the meniscus is that the surface energy is higher at the exposed cracks than at the fluoro-silanated oxide layer [22]. This higher surface energy would require more work to separate the array from the exposed surface of the cracks. However, a more likely explanation is that the trailing meniscuses are due to cracks that open during the curing process and allow uncured PDMS to flow into them, forming covalent bonds with the newly exposed PDMS. These stronger bonds require significantly more work to break them in order to separate the array from the negative mold. Additionally, this explanation is supported by observations of mirrored features of the cracks in the post arrays and the negative molds seen under phase contrast (white arrowheads, figure 6(*b*)). Thus, the large strain energy of the trailing meniscus and the replicated crack-like features in the nanopost arrays indicates that fracture occurs prior to the peeling process.

Thermal fracture in circular PDMS samples

To examine whether thermal expansion is sufficient to induce cracking, test samples were cut from PDMS, oxidized in plasma to form the brittle silica-like layer, and then subjected to two different elevated temperatures to cause thermal expansion (figure 7). Cracks on the surface of the test samples were seen to form a pattern of concentric circles. Higher densities of cracks were at the perimeter of the samples in comparison to the centers of the samples. Phase contrast microscopy of the cracks that formed at the perimeter revealed that the cracks were more pronounced and abundant when the samples were heated to the higher temperature (figures 8(*a*) and (*b*)). At the higher temperature, there was an increased occurrence of cracks aligned in the radial direction that connected concentric circles together. Image thresholding was used to produce binary images where the cracks were segmented and could be quantified (figures 8(*c*) and (*d*)). After heating to a temperature of 150 °C, the average crack density within an image was 8.6 ± 1.2% for 4 test samples and 16 images (figure 9). Samples heated to 180 °C had an average crack density of 14.1 ± 1.7%, which was statistically different than those at 150 °C ($p < 0.01$, Student's *t*-test). Thus, the fractures induced by heating the test samples of PDMS with a silica-like layer suggest a direct correlation between change in temperature and crack formation density.

Finite element modeling of thermal fracture

Since surface cracks occur with higher prevalence at elevated temperatures, we examined whether thermally induced stresses are sufficient to overcome the fracture toughness of the silica-like layer. Finite element analyses of the circular test samples with oxidized PDMS were conducted to evaluate the stresses induced during heating (figure 10(*a*)). Under simulated heating, tensile radial stresses were observed in the silica-like layer due to its lower CTE than that of pure PDMS (figure 10(*b*)). We ran simulations where the Young's modulus of the silica-like layer was varied from 10 MPa to 70 GPa and the maximum radial stress increased nonlinearly with its modulus. The maximum radial stress in the silica-like layer was located between 0.4 and 1 mm from the outer edge of the model, which matches the location where surface cracks in the PDMS test samples had the highest occurrence.

The silica-like layer is too thin for its properties to be measured directly so its fracture toughness K is inferred from the results of the finite element analysis. In order for thermal expansion to be sufficient to induce fracture, the critical value of the induced radial stresses σ_T is given by

$$K = F\sigma_T\sqrt{\pi a} \tag{1}$$

where F is the geometric shape factor and a is the length of the pre-crack defect within the structure of the oxidized PDMS [40]. The fracture toughness K of a material under a plane stress condition can be related to the strain energy release rate G by

$$G = K^2/E \tag{2}$$

where E is the material's Young's modulus [40]. For equation (2), the effects of plasticity within PDMS and its brittle silica-like layer are considered to be negligible. An estimate of strain energy release rate of oxidize PDMS has come from one previous study ($G = 0.1$–0.3 J m^{-2}) [33], but the Young's modulus E has been found to have a wide range of values. It has been estimated to be between 11 [34] and 220 MPa [20] from indentation tests and between 15 [30] and 790 MPa [29] from the analysis of buckled films. The variation in the moduli comes mostly from different oxidizing times and conditions in the formation of the silica-like layer. Together, these estimates give the fracture toughness of the silica-like layer to be between 0.001 and 0.015 MPa m$^{\frac{1}{2}}$, which is far lower than values for fused silica, $K = 0.5$ MPa m$^{\frac{1}{2}}$, and more closely resembles the toughness of organo-silicate glass, $K =$ 0.01–0.05 MPa m$^{\frac{1}{2}}$ [41].

To examine the thermally induced fracture mechanics given by equation (1), we estimated the length of the pre-crack defects to be 10 nm, since nanoparticles of this size are able to diffuse through pores within PDMS [42, 43]. Since the pre-crack defects are much smaller than the thickness of the silica-like layer, the geometric shape factor can be assumed to be unity ($F = 1$). If a fracture toughness of 0.001 MPa m$^{\frac{1}{2}}$ is assumed, then a thermal stress greater than 5 MPa would cause fracture. Given the results of the finite element simulation, this would require that the Young's modulus of the silica-like layer be greater than 100 MPa in order for fracture to occur in the test samples ($\Delta T = 160$ K) and 190 MPa for fracture to occur during casting ($\Delta T = 90$ K). Likewise, if the silica-like layer has a higher fracture toughness ($K = 0.01$ MPa m$^{\frac{1}{2}}$), then its Young's modulus needs to be greater than 1.2 and 2.5 GPa, respectively. Thus, our estimations indicate that CTE mismatch can cause fracture in oxidized PDMS and that its Young's modulus is on the higher end of values previously reported.

Conclusion

With this study we have addressed the possibility that thermal stresses play a significant role in surface crack formation on plasma-oxidized PDMS negative molds during soft lithography replication. Negative molds are subjected to both mechanical and thermal stresses during the fabrication of nanopost arrays. To evaluate the effect of only thermal strains, studies on thermal expansion were conducted without any mechanical factors from peeling or geometry of the array. These studies show that the high CTE of PDMS causes the underlying layer to exert tensile stresses on the less-compliant, silica-like layer. It is likely that within the oxidized PDMS, there is a distribution in the size of pre-crack defects (a in equation (1)). At the lower temperatures, the corresponding tensile stress would be strong enough to cause fracture in only the largest pre-crack defects. At the highest temperature we examined (180 °C), the tensile stress would be strong enough to fracture both the large and small pre-crack defects and thereby lead to the observed increase in crack density with elevated temperatures.

This work shows that surface cracks are a concern in the manufacturability of nanopost arrays because the cracking leads to missing posts. Double-casting is helpful in having one master template for the post arrays that is then replicated into many substrates for biological experiments. It is also cost effective, more efficient, and less wasteful to the environment to reuse the negative molds. However, the wear on the negative molds increases with each casting and undermines the nanoscale pattern fidelity of the replication process. To mitigate the wear, we recommend using lower temperatures during the manufacturing process to reduce the thermally induced stresses. Each negative mold should only be used for a few replications of the arrays before discarding it. Direct-casting of PDMS into a master template of holes is a faster process that is mostly fracture free since it does not require plasma treatment, but it is also susceptible to degradation of the expensive silicon molds when PDMS becomes stuck in the holes.

While the scope of our findings pertains mostly to the fabrication of the nanopost arrays, oxidized PDMS has widespread use in modifying the surface chemistry of PDMS for functionalization or bonding layers of PDMS together to form microfluidic channels. Most of the assays or applications associated with PDMS devices are conducted at room temperature, but in some instances, elevated temperatures are used, e.g., polymer chain reactions or thermal micropumps. The thermal degradation of the silica-like layer on PDMS can be detrimental to the usefulness and reliability of these devices.

Acknowledgments

We thank Corey Pollock and Mamidala Ramulu for helpful discussions and assistance and appreciate the generosity of Ana Wieman and the UW Engineering Undergraduate Research Program. This work was supported in part by funds from the National Science Foundation's Research Experience for Undergraduates (WT), the NSF CAREER Award, and the National Institutes of Health (HL097284).

References

[1] Xia Y N and Whitesides G M 1998 Soft lithography *Angew. Chem. Int. Ed.* **37** 551–75
[2] Whitesides G M, Ostuni E, Takayama S, Jiang X and Ingber D E 2001 Soft lithography in biology and biochemistry *Annu. Rev. Biomed. Eng.* **3** 335–73
[3] McDonald J C, Duffy D C, Anderson J R, Chiu D T, Wu H, Schueller O J and Whitesides G M 2000 Fabrication of microfluidic systems in poly(dimethylsiloxane) *Electrophoresis* **21** 27–40
[4] Sia S K and Whitesides G M 2003 Microfluidic devices fabricated in poly(dimethylsiloxane) for biological studies *Electrophoresis* **24** 3563–76

[5] Quake S R and Scherer A 2000 From micro- to nanofabrication with soft materials *Science* **290** 1536–40

[6] Ruiz S A and Chen C S 2007 Microcontact printing: a tool to pattern *Softw. Matter* **3** 168–77

[7] Sniadecki N J, Desai R A, Ruiz S A and Chen C S 2006 Nanotechnology for cell-substrate interactions *Ann. Biomed. Eng.* **34** 59–74

[8] Lee J N, Jiang X, Ryan D and Whitesides G M 2004 Compatibility of mammalian cells on surfaces of poly(dimethylsiloxane) *Langmuir* **20** 11684–91

[9] Gomez-Sjoberg R, Leyrat A A, Pirone D M, Chen C S and Quake S R 2007 Versatile, fully automated, microfluidic cell culture system *Anal. Chem.* **79** 8557–63

[10] Tan J L, Tien J, Pirone D M, Gray D S, Bhadriraju K and Chen C S 2003 Cells lying on a bed of microneedles: an approach to isolate mechanical force *Proc. Natl Acad. Sci. USA* **100** 1484–9

[11] du Roure O, Saez A, Buguin A, Austin R H, Chavrier P, Siberzan P and Ladoux B 2005 Force mapping in epithelial cell migration *Proc. Natl Acad. Sci. USA* **102** 2390–5

[12] Yang M T, Sniadecki N J and Chen C S 2007 Geometric considerations of micro- to nanoscale elastomeric post arrays to study cellular traction forces *Adv. Mater.* **19** 3119–23

[13] Liang X M, Han S J, Reems J A, Gao D and Sniadecki N J 2010 Platelet retraction force measurements using flexible post force sensors *Lab Chip* **10** 991–8

[14] Grzybowski B A, Brittain S T and Whitesides G M 1999 Thermally actuated interferometric sensors based on the thermal expansion of transparent elastomeric media *Rev. Sci. Instrum.* **70** 2031–7

[15] Govindaraju A, Chakraborty A and Luo C 2005 Reinforcement of PDMS masters using SU-8 truss structures *J. Micromech. Microeng.* **15** 1303–9

[16] Kunnavakkam M V, Houlihan F M, Schlax M, Liddle J A, Kolodner P, Nalamasu O and Rogers J A 2003 Low-cost, low-loss microlens arrays fabricated by soft-lithography replication process *Appl. Phys. Lett.* **82** 1152–4

[17] Fuard D, Tzvetkova-Chevolleau T, Decossas S, Tracqui P and Schiavone P 2008 Optimization of poly-di-methyl-siloxane (PDMS) substrates for studying cellular adhesion and motility *Microelectron. Eng.* **85** 1289–93

[18] Khanafer K, Duprey A, Schlicht M and Berguer R 2009 Effects of strain rate, mixing ratio, and stress-strain definition on the mechanical behavior of the polydimethylsiloxane (PDMS) material as related to its biological applications *Biomed. Microdevices* **11** 503–8

[19] Lotters J C, Olthuis W, Veltink P H and Bergveld P 1997 The mechanical properties of the rubber elastic polymer polydimethylsiloxane for sensor applications *J. Micromech. Microeng.* **7** 145–7

[20] Bar G, Delineau L, Hafele A and Whangbo M H 2001 Investigation of the stiffness change in, the indentation force and the hydrophobic recovery of plasma-oxidized polydimethylsiloxane surfaces by tapping mode atomic force microscopy *Polymer* **42** 3627–32

[21] Sniadecki N J and Chen C S 2007 Microfabricated silicone elastomeric post arrays for measuring traction forces of adherent cells *Methods Cell Biol.* **83** 313–28

[22] Chaudhury M K and Whitesides G M 1991 Direct measurement of interfacial interactions between semispherical lenses and flat sheets of poly(dimethylsiloxane) and their chemical derivatives *Langmuir* **7** 1013–25

[23] Chaudhury M K and Whitesides G M 1992 Correlation between surface free-energy and surface constitution *Science* **255** 1230–2

[24] Duffy D C, McDonald J C, Schueller O J A and Whitesides G M 1998 Rapid prototyping of microfluidic systems in poly(dimethylsiloxane) *Anal. Chem.* **70** 4974–84

[25] Grzybowski B A, Haag R, Bowden N and Whitesides G M 1998 Generation of micrometer-sized patterns for microanalytical applications using a laser direct-write method and microcontact printing *Anal. Chem.* **70** 4645–52

[26] Miller D C, Thapa A, Haberstroh K M and Webster T J 2004 Endothelial and vascular smooth muscle cell function on poly(lactic-co-glycolic acid) with nano-structured surface features *Biomaterials* **25** 53–61

[27] Owen M J and Smith P J 1994 Plasma treatment of polydimethylsiloxane *J. Adhes. Sci. Technol.* **8** 1063–75

[28] Befahy S, Lipnik P, Pardoen T, Nascimento C, Patris B, Bertrand P and Yunus S 2010 Thickness and elastic modulus of plasma treated PDMS silica-like surface layer *Langmuir* **26** 3372–5

[29] Bowden N, Huck W T S, Paul K E and Whitesides G M 1999 The controlled formation of ordered, sinusoidal structures by plasma oxidation of an elastomeric polymer *Appl. Phys. Lett.* **75** 2557–9

[30] Efimenko K, Rackaitis M, Manias E, Vaziri A, Mahadevan L and Genzer J 2005 Nested self-similar wrinkling patterns in skins *Nature Mater.* **4** 293–7

[31] Huh D, Mills K L, Zhu X, Burns M A, Thouless M D and Takayama S 2007 Tuneable elastomeric nanochannels for nanofluidic manipulation *Nat. Mater.* **6** 424–8

[32] Zhu X Y, Mills K L, Peters P R, Bahng J H, Liu E H, Shim J, Naruse K, Csete M E, Thouless M D and Takayama S 2005 Fabrication of reconfigurable protein matrices by cracking *Nat. Mater.* **4** 403–6

[33] Mills K L, Zhu X Y, Takayama S C and Thouless M D 2008 The mechanical properties of a surface-modified layer on polydimethylsiloxane *J. Mater. Res.* **23** 37–48

[34] Hillborg H, Tomczak N, Olah A, Schonherr H and Vancso G J 2004 Nanoscale hydrophobic recovery: a chemical force microscopy study of UV/ozone-treated cross-linked poly(dimethylsiloxane) *Langmuir* **20** 785–94

[35] Hillborg H and Gedde U W 1998 Hydrophobicity recovery of polydimethylsiloxane after exposure to corona discharges *Polymer* **39** 1991–8

[36] Song J, Tranchida D and Vancso G J 2008 Contact mechanics of UV/ozone-treated PDMS by AFM and JKR testing: mechanical performance from nano- to micrometer length scales *Macromolecules* **41** 6757–62

[37] Callister W D 2007 *Materials Science and Engineering: An Introduction* 7th edn (New York: Wiley)

[38] Kobayash A S, Wade B G and Maiden D E 1972 Photoelastic investigation on crack-arrest capability of a hole *Exp. Mech.* **12** 32–7

[39] Murphy D B 2001 *Fundamentals of Light Microscopy and Electronic Imaging* (New York: Wiley)

[40] Dowling N E 2007 *Mechanical Behavior of Materials: Engineering Methods for Deformation, Fracture, and Fatigue* 3rd edn (Upper Saddle River, NJ: Pearson/Prentice Hall)

[41] Volinsky A A, Vella J B and Gerberich W W 2003 Fracture toughness, adhesion and mechanical properties of low-k dielectric thin films measured by nanoindentation *Thin Solid Films* **429** 201–10

[42] Roman G T and Culbertson C T 2006 Surface engineering of poly(dimethylsiloxane) microfluidic devices using transition metal sol–gel chemistry *Langmuir* **22** 4445–51

[43] Roman G T, Hlaus T, Bass K J, Seelhammer T G and Culbertson C T 2005 Sol–gel modified poly(dimethylsiloxane) microfluidic devices with high electroosmotic mobilities and hydrophilic channel wall characteristics *Anal. Chem.* **77** 1414–22